Design, Prototyping, and Evaluation of a Concept for a Shape-Changing Smart Material Building Surface Tile

Robert J. Zupan, Dale T. Clifford, Richard V. Beblo, and John C. Brigham

July 14, 2020

Abstract

A design concept for shape-changing smart material tiles for applications in environmentally responsive building facades is presented. In particular, the application considered is a tile that would change the shape of the building surface to favorably affect the interaction with solar irradiance. A lab-scale prototype system for smart material tiles composed of 3D printed thermally responsive shape memory polymer (SMP) and utilizing localized thermal material activation and uniform pressure actuation is examined. Tests utilizing the prototype tile are used to create and validate a computational (finite element) representation of the adaptive surface tile system. Towards developing this computational representation, a strategy is presented to determine and validate the material parameters for the 3D printed SMP by matching the tile shape predicted by the numerical model to the tile shape measured experimentally. This numerical representation was then implemented into a computational approach to explore the design space for this adaptive tile to have an effect on the solar irradiance on a building surface. More specifically, a series of numerical examples are considered that determine the location and size of material activation that minimize the area of the tile exposed to solar irradiance. Results indicate that the adaptive tile can change the surface of a structure to considerably improve the structure's interaction with solar irradiance. Additionally, the importance of the control strategy for a multi-tile system was displayed, particularly with respect to the capability to significantly reduce the energy cost and affect the solar irradiance to a higher degree by accounting for neighboring tile interaction.

1 Introduction

Energy consumption in the United States is dominated by the commercial building sector at 40% of total energy, and within the commercial building sector the main consumers are lighting and HVAC systems [1]. Due to this, there has been a considerable effort in recent research to reduce energy demand in commercial buildings. Specifically, many of these efforts focus on allowing the building to adapt to internal and external stimuli. Examples of interior building technologies include reducing energy consumption with occupancy sensors for light control [2], or predictive control for ventilation and HVAC systems [3]. Recently, focus has begun to switch to external building technologies, and an example of which is responsive building skins, which change configuration based on an environmental stimulus [4–7].

Responsive building skins have been recently developed to reduce the energy consumption of all main energy consumers within commercial buildings [8]. In an effort to reduce HVAC demand within Media-TIC building in Barcelona an inflatable skin was implemented that inflates portions of the skins based on light sensors to increase insulation [4]. Alternatively the Heliotrace system [4] and the responsive building skin of the Al Bahard towers [5] utilized a series of mechanical apertures to

control the flow of light into their respective buildings. Even more recent work has been considering the possibility of including a variety of smart material technologies to further expand the potential capabilities of responsive building skin technologies. The use of smart materials has several potential benefits, due to their controllable (i.e., programmable) intrinsic property changes and the ability to use naturally occurring stimulus (e.g., heat or solar radiation) or minimal supplied energy to elicit these property changes. Utilizing one or both of these smart material capabilities can lead to smart components that have more adaptivity and/or require less energy to achieve the same level of adaptivity, while also potentially eliminating overall system complexity (e.g., removing the need for hinges, etc.).

There are several smart material technologies that have been implemented into external building structures in order to mechanically change the façade, similar to the example of the Al Bahard towers [5], to allow the building to positively interact with environmental stimuli. For example, in [9] shape memory alloy actuators that were activated when the external temperature reached a predefined level were used to deform portions of a façade. Specifically, portions of the façade would create openings for increased airflow, and would then close once the temperature decreased below the activation threshold. Some examples have constructed environmentally responsive façade components that were instead comprised entirely of smart material, rather than just attaching smart material components to a standard material façade element [6, 7, 10]. A specific example of a façade component comprised of a smart material was explored in [6] which utilizes hygromorphic materials, which behave similarly to a conifer cone in nature when the relative humidity changes [6]. This allows the façade component to "close" and provide shelter during high moisture loads (i.e., rain) and "open" to allow solar exposure during low moisture loads. Alternatively, Barrett et al. developed a building skin that used bimetal sheet layers that had differing coefficients of thermal expansion in order to curl towards or away from the structure based on the thermal loading in the surrounding environment [7, 10]. The curling behavior of the façade component reduced solar gains by providing shading during high thermal loading and increased insulation during periods of low thermal loading. These examples where the façade components are comprised of the smart material themselves, as well as the majority of applications of smart materials within building façade systems in general, have used naturally occurring stimulus alone to illicit the adaptivity. The primary benefit of using naturally occurring stimulus is that no additional energy is required to activate the system. Although, this means that the system is entirely dependent on the environment, which is an issue if the desired behavior is not perfectly correlated with an environmental stimulus.

There have been several applications of smart materials for structures and structural components where active activation (i.e., energy from a man-made source) was used, rather than activation from the natural environment, and the overall performance of the structure still improved [11–16]. One example within building structures involved piezoceramic smart materials [16], which produce an electric charge when subjected to a stress or strain (and the converse effect). In this example, thin wafer piezoceramic sensors were placed (singly or stacked) on a structure to first determine vibrations based on electricity output, and then electrically activated to dampen the vibrations. Additionally, several examples of structures utilizing active smart material activation are present in aeronautical applications [11–15]. For example, actively activated smart material actuators were used to change the shape of wings or blades based on flight plans which allowed aircraft to efficiently adapt to conditions or changes in flight plans (e.g., ascent, descent, increase speed, decrease speed). Utilization of smart materials to change the shape of aircraft wings has simplified the morphing process, resulted in more economic builds, and required less maintenance than previous methods that used standard engineering materials. While active activation does require an additional energy cost, it is an acceptable cost for many applications to allow for more complex behavior of smart material structures. Furthermore, by providing additional functionality it is possible that and the

overall energy savings can be greater with active activation regardless of the cost.

The current study presents a concept for a shape-changing smart material building surface tile that will change shape for optimal interaction with solar exposure. The shape-changing tile façade is entirely comprised of smart material (as opposed to being actuated by smart materials). Active material activation, based on the positioning of the sun, is considered to provide a fully controllable façade with diverse functionality. For the proposed shape-changing tile, the shape-change is achieved through a localized activation of the smart material paired with a uniform pressure to deform the activated ("soft") portion(s) of the tile. The objective of this study is to experimentally and numerically investigate the capabilities of this shape-changing tile concept. As such, a physical prototype of the tile concept was developed using a shape memory polymer as the smart material. This prototype was then used to develop, calibrate, and validate a numerical representation (finite element model) of the tile based on experimental results. A design concept utilizing the numerical representation was developed and evaluated through numerical case studies in the context of reducing the area of a building exterior in solar exposure. It should be noted that this concept is in early development and the focus of this work is primarily on numerically evaluating the feasibility of this concept to have a significant effect on the building-environment interaction. In the following section, details of the benchtop experiments are given, including the manufacturing of the shape memory polymer tiles, the test apparatus setup, experimental procedure, and evaluation of the experimental results. A general computational representation of the smart material building skin tile is developed and presented in Section 3 as well as details on material model calibration and model validation. Numerical examples, their results, and discussion are then given in Section 4, which is followed by concluding remarks in Section 5.

2 Adaptive Smart Material Tile Design Concept

The design concept considered herein is an adaptive shape changing "wrinkled" surface tile based upon the prior work developing building surface "cactus tiles" by Clifford [17]. The original cactus tile objective from the previous work was to have static "wrinkled" surface tiles that were both aesthetically pleasing and had functional benefits in terms of self-shading. However, it is envisioned that adding the capability of such tiles to change between wrinkle patterns, would further enhance the original benefits and potentially include many other functional behaviors [17–19]. The proposed mechanism to produce a tile that can morph between different wrinkle patterns (i.e., shape changing cactus tile) is envisioned to be controllable localized activation of the smart material comprising the tile (e.g., softening) and mechanical actuation to deform the tile into a desired shape. Localized material activation has been shown to improve the efficiency of a shape-changing structure [20] and is utilized as an additional control variable to increase functionality of the shape-changing building surface tile.

2.1 Benchtop Prototype

A physical prototype of the design concept was developed to explore the practical feasibility and provide the experimental results from which to develop a numerical representation for further evaluation. This prototype was developed with a thermally responsive shape memory polymer (SMP) as the smart material. It should be noted that the SMP used for the prototype is not proposed as the preferred material for actual construction, but allowed rapid prototype development and is representative of the morphing capability that would be desired as further development and material selection occurred. The following text details the process to construct and test the morphing capability of the SMP tile.

Figure 1: Printed SMP material.

2.1.1 SMP Tile Printing

The SMP tile was created using 3D printing of a polyurethane filament provided by SMP Technologies Inc. [21]. A standard 3D printer, a Creator Pro Dual Extrusion 3D printer by Flashforge, was used for the printing process. The printing software utilized was Matter Control with settings of infill speed, top solid infill speed, support material speed, and travel speed of 30 mm/s, inside and outside perimeters speeds of 25 mm/s, extruder temperature of 210°C, and bed temperature of 48°C. The resultant tile had an activation temperature, T_g, of 55°C [22, 23]. Figure 1 shows an example of the printed SMP tile material. In particular, it can be seen that the printing process prints alternating layers of horizontal and vertical alignment, which yielded a transversely isotropic overall material behavior. The 3D printed SMP tile was chosen for a number of reasons. First, the 3D printing process was selected as it allowed for a relatively high level of control over the initial shape of the tile in comparison to a casting process. In addition, the printing process also allows for the shape and other parameters of the tile to be changed much more easily than casting, which is a benefit when investigating the potential design space of a device (i.e., being able to switch between designs easily from a fabrication perspective). 3D SMP printing, though tedious, resulted in a less expensive fabrication process in terms of production time and cost in comparison to a casting process. Additionally, the 3D printing process itself avoids many of the issues that can arise while casting a SMP specimen (i.e., bubbles, uneven casting, and leakage). Furthermore, throughout the experimental process the 3D printed specimens exhibited behavior consistent with published SMP behavior regardless of manufacturing approach.

2.1.2 Test Apparatus and Morphing Procedure

Figure 2 shows the apparatus used to test the SMP tiles and evaluate their morph capability, including a breakdown of the apparatus components and dimensions. Acrylic plates were used to frame the tile, with an entry point for pneumatic actuation in the back. This allowed for a uniform pressure to be applied by a compressor to deform the tile following material activation. The SMP tile was bolted into the test jig using 12 #8 machine screws, ensuring an air tight seal. The tile was then actuated through the use of a constant pressure, 10 psi, applied by the compressor. Next, the tile was heated by a Milwaukee Heat Gun (1400 W) until the T_g of 55°C was reached (confirmed

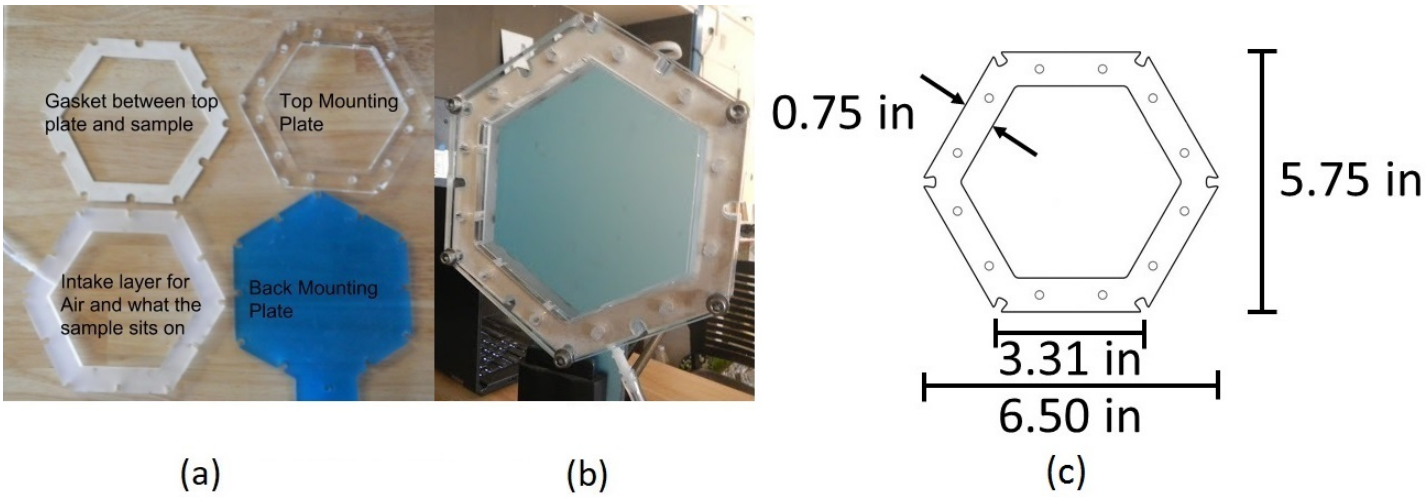

Figure 2: The test apparatus that was used to evaluate the SMP tile morphing, including (a) the layers of the apparatus, (b) the fully assembled apparatus, and (c) the dimensions of the apparatus.

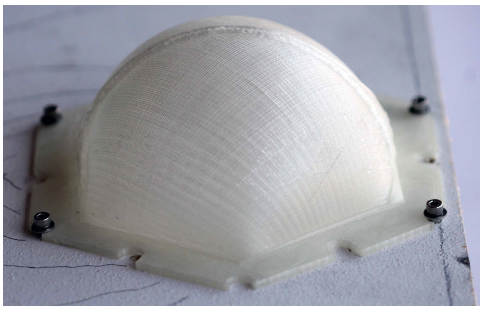

Figure 3: Deformed fully activated SMP tile with uniform pressure.

using a FLIR infrared camera). As the temperature of the SMP rises the stiffness of the material decreases allowing deformation under uniform pressure. The application of uniform pressure was not removed until the tile was cooled and "locked" into place. Photographs of the deformed shape were taken by a digital camera in order to extract the surface deformation for input into solar analysis software and to develop the computational framework.

2.2 Experimental Test Cases

Two experimental tests were performed using the procedure described in Section 2.1.2. In the first experiment, the entirety of the tile was heated to T_g (referred to as "fully activated"). Figure 3 shows an example of the deformed shape of the fully activated tile. This morphed fully activated tile had an expected rotationally symmetric positive Gaussian curvature "hemispherical" shape. In the second experiment the heat gun was localized to a single location on the tile, resulting in an approximately circular portion of the tile being activated (referred to as "locally activated"). The locally activated tile with constant pressure resulted in an asymmetric deformed tile shape. The resultant deformation of these tiles, both fully and locally activated, was found to be recoverable and repeatable without any indications of damage.

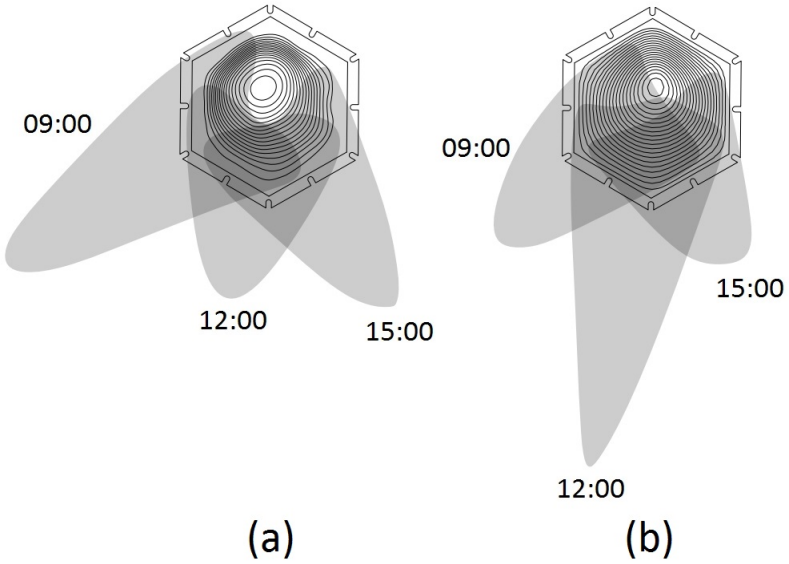

Figure 4: Shading profiles for the (a) fully activated and (b) locally activated tiles at 09:00, 12:00, and 15:00 on June 21^{st} 2015.

2.3 Shading Potential of Deformed SMP Tiles

Although a more refined evaluation of the design concept was performed using a numerical representation, the experimental results from the prototype were used to perform a preliminary evaluation of the self shading potential of the design concept, particularly the use of localized activation to affect the amount of self-shading with respect to the position of the sun. Specifically, the shading profile of both the fully and locally activated tiles, as if they were vertically mounted on an unobstructed South facing wall, were determined for three times on June 21^{st} 2015: 09:00, 12:00, and 15:00. The shading profiles were determined using Rhinoceros 3D [24] with time, date, location, and an object file (i.e., the deformed shape of the tile) as input. The shape of the fully activated tile was held constant for all three times, whereas, the shape of the locally activated tile was changed by rotating the tile so that the peak of the deformed shape was in-line with the position of the sun and the center of the tile. Figure 4 shows the shadow cast by the morphed tile for both fully activated and locally activated cases, noting that the locally activated case had a different location of activation for each of the three time points. For all times both the fully and locally activated tiles provided significant self-shading, as well as shading beyond the boundaries of the tile. Specifically, the location of material activation in the locally activated tile had a large effect on the shadow cast in comparison to the fully activated tile. Moreover, the locally activated tile requires less activation energy than the fully activated tile thereby reducing overall energy costs of the system.

3 Computational Smart Material Tile Representation

Utilizing the observations from the physical experiments with the benchtop prototype, a numerical representation of the smart material tile was developed with standard finite element analysis. Figure 5 shows a schematic of the tile and the parameters defining material activation. The numerical representation of the tile was defined with the same dimensions as those shown in Figure 2(c) with a thickness of 0.1 in. The shape changing process was assumed to be quasi-static. The outer 0.75 in were taken to be fixed with zero displacement in all directions, while all other faces were free to

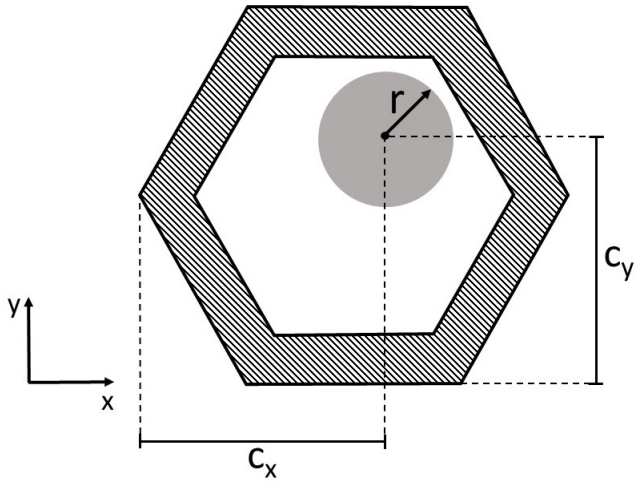

Figure 5: Schematic of the tile concept where activated material is gray and unactivated material is white.

deform due to the actuation pressure being applied (similar to the experimental case a pressure of 10 psi was used). The geometry was meshed with TET10 elements and the mesh was refined until convergence was assured. The material was assumed to be instantaneously activated so that regions of the tile were either activated or inactivated completely (i.e., no transition zones). Specifically, the material was activated in the model by simply switching the modulus of activated elements to the determined value of the activated modulus. The deformation was assumed to be quasi-static and the analysis was nonlinear in both geometry and material. The SMP tile was assumed to be an isotropic Neo-Hookean hyperelastic material with a fixed Poisson's ratio of 0.45 (i.e., nearly incompressible). The assumption of isotropy, even though the material is truly transversely isotropic, was used due to the forces being applied in the out of plane direction causing membrane behavior to dominate the response of the system. The Young's modulus of the unactivated tile material (i.e., glassy modulus) was observed to have a minimal effect on the deformed tile shape (provided it was sufficiently higher than the Young's modulus of the activated tile material). Therefore, the glassy modulus was fixed at a value of 150 ksi based on the reported literature [23]. Most importantly, for the finite element analysis to be representative of the experimental prototype it was necessary to estimate the activated tile Young's modulus and validate the assumption of the circular activated region based on the experimental results. It should be noted the numerical determination of the activated tile Young's modulus was required due to experimental limitations that did not allow for material characterization.

3.1 Calibration and Validation Procedure

The calibration and validation of the numerical representation of the smart tile was performed using an optimization-based inverse problem solution strategy based on the work in [18, 19]. The inverse problem was to estimate the unknown tile material parameters and the activated material distribution to match the shape of the tile measured through the associated experimental test of the prototype. Therefore, the inverse problem could be cast as the following constrained optimization

problem:

$$\begin{aligned} \underset{\vec{\gamma}}{\text{minimize:}} \quad & MH_d\left(S_T, S_F(\vec{u})\right) \\ \text{subject to:} \quad & F(\vec{u}, \vec{\gamma}) = 0 \\ & \vec{b}_l \leq A(\vec{\gamma}) \leq \vec{b}_u, \end{aligned} \tag{1}$$

where S_T is the target surface shape, S_F is the predicted morphed shape of tile as defined by the deformation of the tile, $\vec{u}$, estimated by the finite element analysis of the forward problem (FEBio software, with standard TET10 elements), $F(\vec{u}, \vec{\gamma}) = 0$ (i.e., the partial differential equation constraint), for a given set of parameters, $\vec{\gamma}$ (which will be defined in the respective cases), $MH_d(\cdot, \cdot)$ is the metric that quantifies the difference between two shapes, $\vec{b}_l$ and $\vec{b}_u$ are the lower and upper bound constraint vectors, respectively, and $A(\vec{\gamma})$ is the operator that forms the necessary constraint equations involving the activation parameters. The metric to quantify the difference between two shapes, $MH_d(\cdot, \cdot)$, was the Modified Hausdorff distance [25]. This metric was chosen due to positive results in previous work [18] in matching a shape changing tile model to a predefined target shape. The Modified Hausdorff distance is calculated for two discretized shapes, S_1 and S_2, as:

$$MH_d(S_1, S_2) = \max(M(S_1, S_2), M(S_2, S_1)) \tag{2}$$

where:

$$M(S_1, S_2) = \frac{1}{N_1} \sum_{i=1}^{N_1} \min_{\vec{x_2} \in S_2} \parallel \vec{x_1}_i - \vec{x_2} \parallel, \tag{3}$$

$\vec{x_1}$ and $\vec{x_2}$ are the Euclidean coordinates of the i^{th} points on shapes S_1 and S_2, respectively, N_1 is the total number of points on S_1, and $\parallel \cdot \parallel$ is the standard Euclidean distance. This Modified Hausdorff distance is analogous to an L_2 norm and ensures that every point on each shape contributes to the distance metric [25].

A standard gradient-based interior point optimization algorithm [26] was utilized. For each inverse solution estimation, the gradient-based optimization was repeated ten times, with a new randomly generated initial solution guess each time. The stopping criteria for each optimization process was set to be when the change in objective function between iterations fell below a tolerance value of 10^{-6}. The final estimate for the inverse solution was then chosen as the result out of the ten with the lowest Modified Hausdorff distance value.

3.1.1 Calibration and Validation Results

First, the unknown Young's modulus of the activated SMP tile was determined by applying the inverse solution procedure to the test results for the case with the fully activated tile. Therefore, $\vec{\gamma}$ is the Young's modulus of the activated material ($\gamma = E_T$). The result of the inverse solution estimation for all ten random starting points (approximately 0.1% difference between solutions) was a Young's modulus of approximately 341 *psi*. The Modified Hausdorff distance between the deformed tile surface estimated by the finite element model with the inverse solution for Young's modulus and the surface extracted from the experiment was 0.148 *in*. A 3D plot and cross-sectional view of the deformed tile surface estimated by the finite element model with the inverse solution for Young's modulus and the surface extracted from the experiment can be seen in Figure 6. This Modified Hausdorff distance that was less than 3% of the tile height was deemed to be sufficiently accurate, and thus, the inverse solution for the Young's modulus was sufficiently accurate.

The activated Young's modulus value found was used in the proceeding test to determine the accuracy of the localized material activation design variable parameterization. For the second test

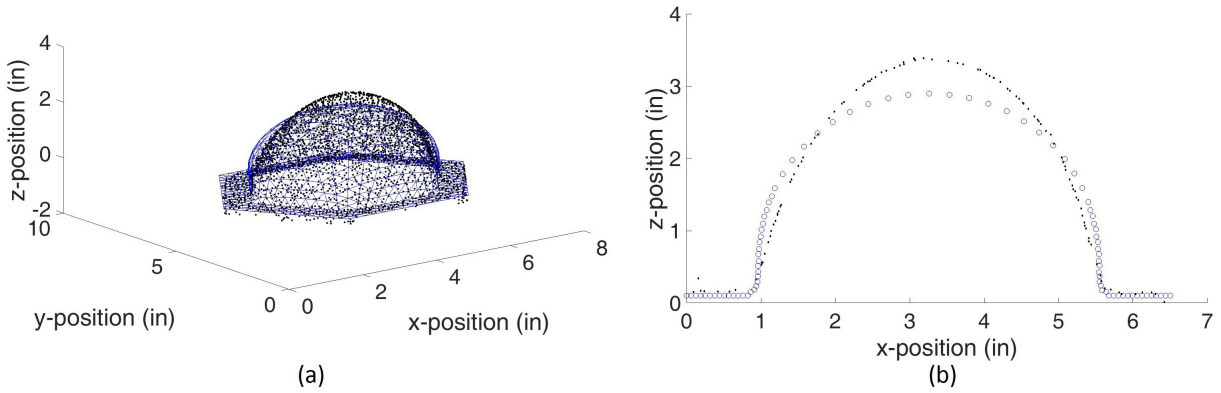

Figure 6: A (a) 3D view and (b) cross-sectional view (taken at $y = 0$) of the extracted surface of the fully activated experimental tile (blue) and the surface extracted from the model with the estimated Young's modulus (black).

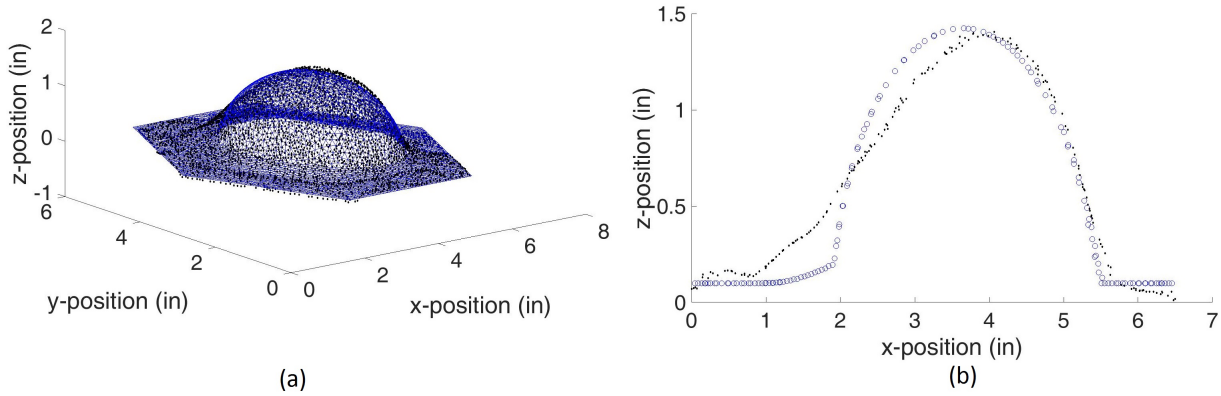

Figure 7: A (a) 3D view and (b) cross-sectional view (taken at $y = 0$) of the extracted surface of the locally activated experimental tile (blue) and the surface extracted from the locally activated tile model (black).

the Young's modulus of the activated material is known, therefore the variable $\vec{\gamma}$ is set equal to the activation parameters ($\vec{\gamma} = \{c_x, c_y, r\}$), where c_x is the x-coordinate of the center of activation, c_y is the y-coordinate of the center of activation, and r is the radius of activation (as shown in Figure 5). The solution for all ten random starting points resulted in a Modified Hausdorff distance between the deformed tile surface estimated by the finite element model and the surface extracted from the locally activated tile experiment of 0.09 in, which was judged to be sufficiently accurate (less than 2% of the tile height). A 3D plot and cross-sectional view of the deformed tile surface estimated by the finite element model and the surface extracted from the experiment can be seen in Figure 7. The material activation parameters for the optimal solution were the center point of activation being located at ($3.74\ in, 3.11\ in$) and the radius of activation being 1.89 in. This solution results in the upper right-hand quadrant of the tile being activated which is consistent with the location of activation in the experimental tile.

As stated previously, the preliminary goal of this design concept was to increase the shaded area of the building envelope (or reduce the area in solar exposure). In order to determine if the numerical representation was accurately representing the design concept, the shading potential of the extracted surface of the locally activated experimental tile and the resultant surface of

the numerical tile must be determined. To compare the extracted experimental surface and the resultant surface from the numerical representation for the locally activated tile an algorithm that was developed and validated with experimental data in [19] was used to determine the percentage of shaded area for these two surfaces on July 21^{st}, 2015. The extracted experimental surface resulted in 35.4% of the tile surface area in shade, while the resultant surface from the numerical representation resulted in 32.6% of the tile surface area in shade. This difference in shaded area was judged to be within acceptable limits, which indicated that the model accurately represented the design concept and could be used to explore the potential capabilities further.

4 Self-Shading Capability of the Smart Material Building Surface Tile

The validated numerical representation was utilized to investigate the potential capabilities of the adaptive self-shading smart material design concept through a series of numerical case studies. These case studies were intended to investigate not just the self-shading capability of the design concept, but also implementational aspects, including the frequency of morphing (e.g., hourly, daily, or monthly shape changes) and the interaction of neighboring tiles if installed as an array (as opposed to a singular tile). A computational design optimization procedure was applied to each test case to determine the size and location of the circular region of localized activation to minimize the area of the tile exposed to solar irradiance. This design optimization utilized the same procedure as was used for the inverse solution estimation described in Section 3, with the exception of the objective function. The objective function in Equation 1 was replaced for the optimal design process with the following:

$$\underset{\gamma}{\text{minimize:}} \quad \sum_{i=1}^{n_t} E_A\left(t_i, S_F(\vec{u})\right) \tag{4}$$

where n_t is the number of times used to estimate solar exposure, t_i is the i^{th} time of interest, and $E_A(\cdot,\cdot)$ is the metric that quantifies the area exposed to solar irradiance for the given tile shape and dependent upon the chosen date, geographic location (latitude and longitude), vertical location, and tile orientation (again, this was calculated using the algorithm from [19]). The same optimization method used in Section 3.1 was used for this problem as well. Minimizing the area of the tile exposed to solar irradiance was chosen as an objective due to the relationship between temperature, radiated energy, and conducted energy, even though this would increase the temperature of the areas exposed. As the temperature of a smaller area increases it also increases the energy radiated off of the surface rather than being conducted into the building. For all the proceeding tests it was assumed that the theoretical tiles were vertically mounted on an unobstructed South facing wall in Phoenix, Arizona (latitude of 33.45° and longitude = −112.07°, with positive latitude being North and positive longitude being East). A final important consideration not yet mentioned for the design of this type of smart material shape changing structure is to ensure that the design solution does not damage the structure. Although a constraint could be included in the design optimization problem to prevent solutions that damage the material [20], preliminary tests showed this to be unnecessary for the case studies considered. However, the final design solutions were still checked to ensure no damage of the material would occur by confirming the maximum principal strain anywhere in the deformed SMP tiles did not exceed damage limits of 30% for inactivated material or 400% for activated material. Finally, it should be noted that an iterative procedure (combination of computational mechanical representation of the tile and numerical optimization) continued to be used due to the fact that, similar to the prior inverse characterization problem, a

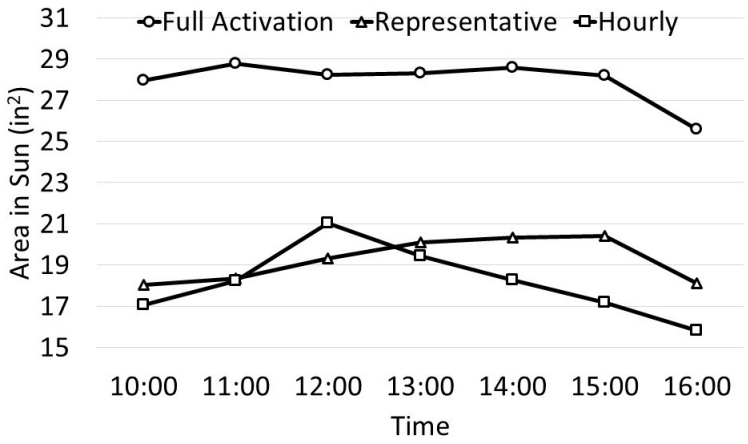

Figure 8: Area of solar exposure with respect to time for the fully activated tile (circle), daily optimized tile (triangle), and hourly optimized tile (square).

direct solution to the optimal design inverse problem is not tractable.

4.1 Numerical Case Studies for a Single Tile

For the single tile numerical case studies, the focus was to determine the effect of different morphing frequencies. Specifically, hourly, daily, and monthly morphing frequencies were considered. For this first case study the area of tile exposed to solar irradiance was calculated for the timespan of 10:00-16:00 on July $21^{st}, 2015$ for three different tile control methods. The first control method was a tile that does not change (i.e., a static tile) that has the shape of the fully activated tile from the previous investigation (Figure 6) (referred to as "fully activated tile"). The second control method was a tile that does not change (i.e., a static tile) that has a shape that minimizes the area of tile that is exposed to solar irradiance for the summation of three representative times of the day ($n_t = 3$) of interest (10:00, 12:00, and 14:00) (referred to as "representative tile"). The final control method was a tile that changed hourly (i.e., a dynamic tile) to the shape that minimized the area of the tile that was exposed to solar irradiance at the beginning of the hour ($n_t = 1$) of interest (referred to as "hourly tile"). Figure 8 shows the area of solar exposure for the timespan of 10:00-16:00 for the fully activated tile, the representative tile, and the hourly tile. Specifically, the representative tile and the hourly tile resulted in an average of 31.2% and 35.1% less exposed area, respectively, than the fully activated tile. Additionally, the hourly tile resulted in an average decrease of 5.6% exposed area compared to the representative tile. Furthermore, there is one time point (12:00) where the representative tile results in the least tile area exposed to solar irradiance. This is likely due to the fact that the representative tile shape was optimized to minimize solar exposure for not only this time, but also times around 12:00 as well.

For the second case study the solar exposure was calculated for the timespan of 10:00-16:00 on August $21^{st}, 2015$ for three different tile control methods. The first control method was again a tile that does not change (i.e., a static tile) that has the shape of the fully activated tile from the previous investigation (Figure 6) (referred to as "fully activated tile"). The second control method was a tile that does not change (i.e., a static tile) that has a shape that minimizes the area of tile that is exposed to solar irradiance at noon on July $21^{st}, 2015$ (referred to as "July tile"). The final control method was a tile that does not change (i.e., a static tile) that has a shape that minimizes the area of tile that is exposed to solar irradiance at noon on August $21^{st}, 2015$ (referred to as

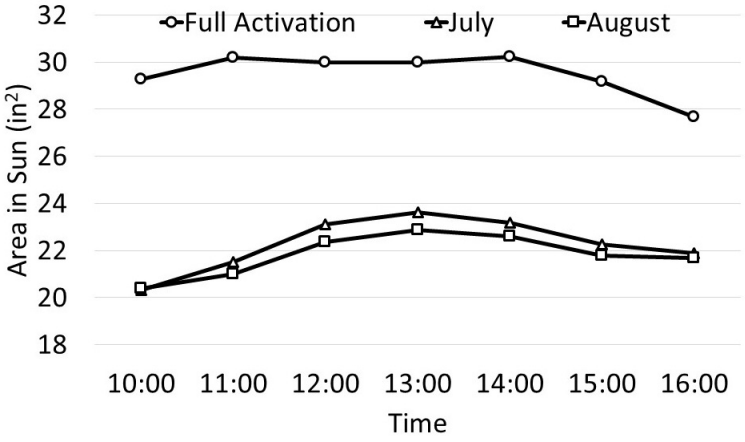

Figure 9: Area of solar exposure with respect to time for the fully activated tile (circle), the tile optimized for noon in July (triangle), and the tile optimized for noon in August (square).

"August tile"). Figure 9 shows the area of solar exposure for the timespan of 10:00-16:00 for the three tile control cases. The July and August tiles resulted in an average of 24.5% and 26.1% less exposed area, respectively, in comparison to the fully activated tile. The August tile resulted in an average decrease of 2.0% exposed area compared to the July tile. These results indicate that increasing the morphing frequency results in a larger decrease in area exposed to solar irradiance. It can also be seen that the closer to winter the date is (the sun has a lower elevation angle) the overall exposed area will increase (the solar angle is closer to the normal of the building surface). Thus, a flat tile is preferred during winter months to minimize the area of the tile exposed to solar irradiance.

4.2 Numerical Case Study for an Array of Tiles

For the final set of numerical case studies, the performance of the tile in an array setting was investigated to assess potential interactions in the shading provided by neighboring tiles and how the control process may be changed due to these interactions. Specifically, a two-by-two array in a "honeycomb" configuration was used, as shown in Figure 10. Similarly to the single tile investigation, the array of tiles was assumed to be mounted onto a South facing wall in Phoenix, Arizona on July 21^{st}, 2015. Four different cases were considered which will be defined by the control method of the array and how the shape of the array was determined. In the first array considered all four tiles were controlled together (i.e, all tiles in the array were the same shape) to take the shape of the fully activated tile from Section 3.1.1 (referred to as "fully activated"). In the second array considered all four tiles were controlled together to take the shape that minimizes the area of a single tile exposed to solar irradiance at 12:00 on July 21^{st}, 2015 (from Section 4.1) (referred to as "dependent control single tile design"). In the third array considered all four tiles were controlled together to take the shape that minimizes the area exposed to solar irradiance for the entire array at 12:00 on July 21^{st}, 2015 (referred to as "dependent control array design"). In the final array considered all four tiles were controlled independently (i.e., potentially four different tile shapes) to take the shape that minimizes the area exposed to solar irradiance for the entire array at 12:00 on July 21^{st}, 2015 (referred to as "independent control array design"). Additionally, for each array of tiles the volume of activated material was calculated as well in order to have an indication of the energy required for the morphing process.

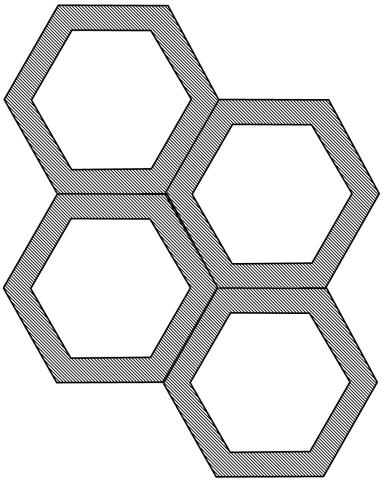

Figure 10: The "honeycomb" arrangement of the array of tiles.

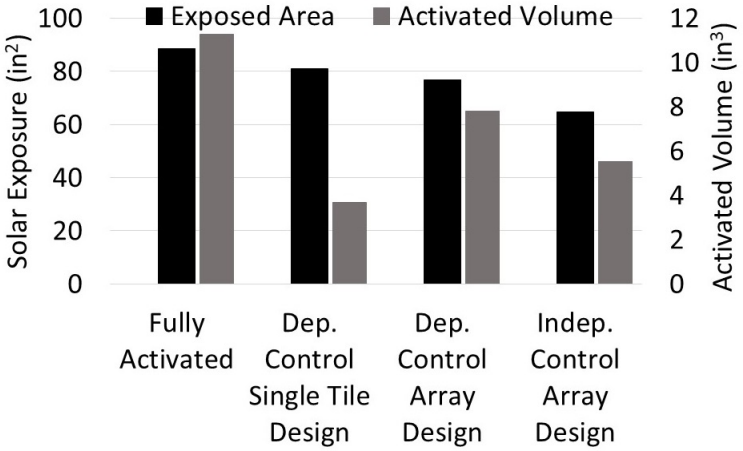

Figure 11: Area of solar exposure and volume of material activation for the fully activated array, dependent control single tile design, dependent control array design, and independent control array design.

Figure 11 shows the area of solar exposure at 12:00 on July $21^{st}, 2015$ and volume of activated material for all four arrays considered. Figure 11 shows that the dependent control array design and independent control array design resulted in less area exposed to solar irradiance than the fully activated array and the dependent control single tile design. Specifically, the dependent control array design resulted in more than 5% decrease in exposed area in comparison to the fully activated array and the dependent control single tile design and the independent control array design resulted in more than 20% decrease in exposed area in comparison to the fully activated array and the dependent control single tile design. This indicates that minimizing the area exposed to solar irradiance for the entire array (as opposed to a singular tile) results in a larger decrease in area exposed to solar irradiance. Additionally, the independent control array design resulted in 15% less exposed area than the dependent control array design, which indicates that controlling the tiles independently (i.e., potentially all different tile shapes), as opposed to controlling the tiles dependently (i.e., all tiles are the same shape), is more beneficial in terms of reducing the area exposed to solar irradiance. In terms of activation volume the independent control array

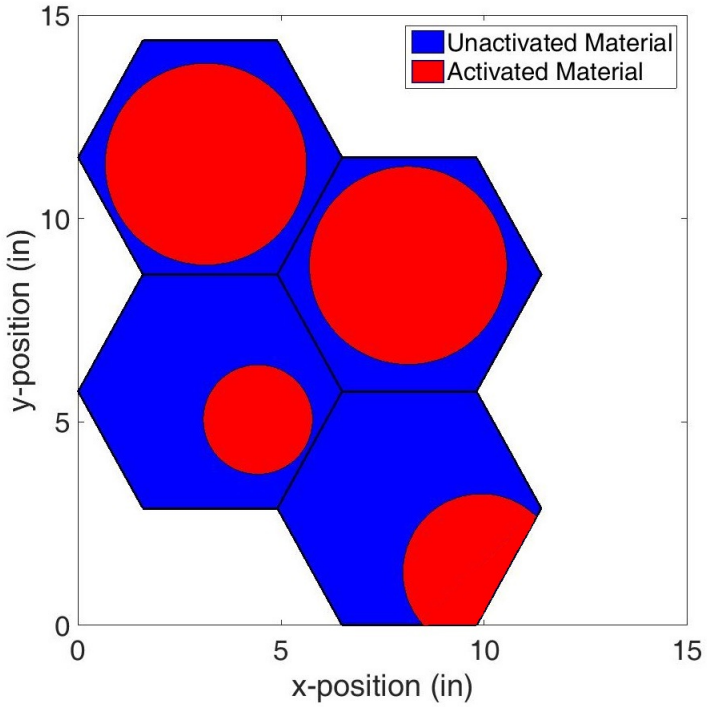

Figure 12: Top view of the unactivated (blue) and activated (red) material for the array of tiles for the independent control array design.

design resulted in 29.2% less activated volume that that of the dependent control array design. As an example, Figure 12 shows the activated material distribution for the independent control array design. The activation is primarily located in the upper tiles of the array. This is due to the optimization of the independent control array design recognizing that tiles closer to the sun provide shading for the subsequent tiles, therefore, the subsequent tiles do not need to be activated to the same extent. This results in a large portion of the array not needing activation thereby reducing the energy required to provide shading for the array of tiles.

5 Conclusions

The design concept of a shape-changing smart material building skin tile was presented in the context of reducing solar irradiance entering a building. The concept was initially explored through experimental tests that explored localized smart material activation. A numerical model of the shape-changing tile was developed, calibrated, and validated based on the experiments and was then implemented within a computational approach with the purpose of designing the morphing mechanisms of the tile. The computational approach for the design of this tile was evaluated through numerical examples that considered the capability of the computational procedure utilizing localized material activation to optimally interact with solar exposure. The results indicated that the design of the physical tile can be accurately represented by the computational approach. Additionally, it was shown that the morphing frequency (i.e., hourly, daily, monthly, etc.) has a significant effect on the area of the tile exposed to solar irradiance. Finally, it was determined that if the tiles are arranged in an array configuration controlling the tiles independently from one another not only leads to less tile area being exposed to solar irradiance but also requires less tile area to be activated.

6 Acknowledgments

The authors gratefully acknowledge the financial support of the National Science Foundation through Award No. 1536797.

References

[1] Renewable Energy. Energy efficiency trends in residential and commercial buildings. 2010.

[2] Marie-Claude Dubois and Åke Blomsterberg. Energy saving potential and strategies for electric lighting in future north european, low energy office buildings: A literature review. *Energy and Buildings*, 43(10):2572–2582, 2011.

[3] Jan Širokỳ, Frauke Oldewurtel, Jiří Cigler, and Samuel Prívara. Experimental analysis of model predictive control for an energy efficient building heating system. *Applied energy*, 88 (9):3079–3087, 2011.

[4] Y Dewidar, N Mohamed, and Y Ashour. Living skins: A new concept of self active building envelope regulating systems. In *Advancing the Green Agenda; Technology, Practices and Policies Conference–BUID*, pages 1–8, 2013.

[5] Karen Cilento. Al bahar towers responsive facade/aedas. *ArchDaily,September*, 5, 2012.

[6] Artem Holstov, Ben Bridgens, and Graham Farmer. Hygromorphic materials for sustainable responsive architecture. *Construction and Building Materials*, 98:570–582, 2015.

[7] Ronald M Barrett and Ronald P Barrett. Thermally adaptive building coverings: Theory and application. In *ASME 2016 Conference on Smart Materials, Adaptive Structures and Intelligent Systems*, pages V002T06A001–V002T06A001. American Society of Mechanical Engineers, 2016.

[8] MA Shameri, MA Alghoul, Kamaruzzaman Sopian, M Fauzi M Zain, and Omkalthum Elayeb. Perspectives of double skin façade systems in buildings and energy saving. *Renewable and Sustainable Energy Reviews*, 15(3):1468–1475, 2011.

[9] Marco Formentini and Stefano Lenci. An innovative building envelope (kinetic façade) with shape memory alloys used as actuators and sensors. *Automation in Construction*, 85:220–231, 2018.

[10] Ronald M Barrett and Ronald P Barrett. Thermally adaptive building covering field test. *Procedia Engineering*, 145:26–33, 2016.

[11] Robert G Loewy. Recent developments in smart structures with aeronautical applications. *Smart Materials and Structures*, 6(5):R11, 1997.

[12] Ermira J Abdullah, Cees Bil, and Simon Watkins. Application of smart materials for adaptive airfoil control. *AIAA paper*, (2009-1359), 2009.

[13] Victor Giurgiutiu. Review of smart-materials actuation solutions for aeroelastic and vibration control. *Journal of Intelligent Material Systems and Structures*, 11(7):525–544, 2000.

[14] S Barbarino, R Pecora, L Lecce, A Concilio, S Ameduri, and L De Rosa. Airfoil structural morphing based on sma actuator series: numerical and experimental studies. *Journal of Intelligent Material Systems and Structures*, 22(10):987–1004, 2011.

[15] Friedrich K Straub and Robert J King. Application of smart materials to control of a helicopter rotor. In *Smart Structures and Materials 1996: Industrial and Commercial Applications of Smart Structures Technologies*, volume 2721, pages 66–78. International Society for Optics and Photonics, 1996.

[16] Gangbing Song, Vineet Sethi, and H-N Li. Vibration control of civil structures using piezoceramic smart materials: A review. *Engineering Structures*, 28(11):1513–1524, 2006.

[17] Dale Clifford. Cactus tile concept, 2019. URL `http://cmubiologic.weebly.com/cactus-tile.html`.

[18] Robert J Zupan, Richard V Beblo, Dale T Clifford, Ankush Aggarwal, and John C Brigham. Design optimization of a self-shading smart material morphing building skin. *Conference on Advanced Building Skins*, 2017.

[19] Robert Joseph Zupan, Dale Clifford, Richard Beblo, and John Brigham. Numerical investigation of capabilities for dynamic self-shading through shape changing building surface tiles. *Journal of Facade Design and Engineering*, 6(1), 2018.

[20] Shuang Wang and John C Brigham. A computational framework for the optimal design of morphing processes in locally activated smart material structures. *Smart Materials and Structures*, 21(10):105016, 2012.

[21] SMPtechno. Shape memory polymer, smp technologies inc., diaplex, 2018. URL `http://www.smptechno.com/index_en.html`.

[22] Jinsong Leng, Xin Lan, Yanju Liu, and Shanyi Du. Shape-memory polymers and their composites: stimulus methods and applications. *Progress in Materials Science*, 56(7):1077–1135, 2011.

[23] Richard Beblo, Korey Gross, and Lisa Mauck Weiland. Mechanical and curing properties of a styrene-based shape memory polymer. *Journal of Intelligent Material Systems and Structures*, 21(7):677–683, 2010.

[24] Robert McNeel et al. Rhinoceros 3d. *Retrieved Jan*, 15, 2009.

[25] M-P Dubuisson and Anil K Jain. A modified hausdorff distance for object matching. In *Pattern Recognition, 1994. Vol. 1-Conference A: Computer Vision & Image Processing., Proceedings of the 12th IAPR International Conference on*, volume 1, pages 566–568. IEEE, 1994.

[26] Donald Goldfarb and Shucheng Liu. An o (n3l) primal interior point algorithm for convex quadratic programming. *Mathematical Programming*, 49(1-3):325–340, 1990.